CONSTRUCTION OF INJECTOR SYSTEM FOR SPring-8 X-FEL

H. Hanaki#, T. Asaka, H. Ego, H. Kimura, T. Kobayashi, S. Suzuki,
JASRI/SPring-8, Hyogo 679-5198, Japan
T. Fukui, T. Inagaki, Y. Kumagai, Y. Otake, T. Shintake, K. Togawa, M. Yamaga ,
RIKEN/SPring-8, Hyogo 679-5198, Japan

Abstract

In design of the XFEL injector, we have emphasized reduction of the emittance growth and enhancement of beam stability. L-band accelerating structures were introduced to decrease the velocity bunching ratio. The accelerating structures are APS type and have been manufactured very precisely not to cause the emittance growth. An L-band waveguide system employs a vacuum type without a circulator and thus it was carefully designed and fabricated to minimize RF reflections to a klystron for its stable operation. RF amplifiers, which adopt thorough countermeasures for RF stabilization and noise reduction, were confirmed to nearly achieve tolerances for the RF stability given by a beam simulation. Deformation of the geomagnetic field was found and then the RC floor in the injector area was demagnetized for a geomagnetic correction magnet to function.

INTRODUCTION

Early in 2007, the construction of the SPring-8 XFEL started aiming at generation of 0.1 nm X-rays, and will be completed by the end of this year [1]. Now an electron gun, accelerating structures and RF power sources of the injector have been almost completed and the installation of them started from the middle of May and will continue until the end of July.

The most remarkable feature of the SPring-8 XFEL is employment of a thermionic gun. This carefully designed therminonic gun can generate a solid cylindrical beam pulse holding uniform charge densities without the nonlinear space charge effect, therefore the initial beam emittance can be as low as the thermal emittance [2]. A thermionic gun injector, however, requires stepwise bunching of an electron beam by means of complex multistage RF cavities not to degrade an initial emittance.

We have emphasized reduction of the emittance growth and enhancement of beam stability in design of the XFEL injector as follows: The injector design is based on the experience of the SCSS test accelerator, however, the velocity bunching ratio is designed to be about 1/5 of that of the SCSS (~100) to suppress the emittance growth as low as possible. Thus we introduced two L-band APS structures instead of the SCSS's S-band structures. Manufacture of the L-band system has been difficult because it employs long APS's precisely machined and a vacuum type waveguide system. In addition, extra RF cavities of 1428 and 5712 MHz will be installed to linearize the bunch compression process to enhance the compression factor.

#hanaki@spring-8.or.jp

The acceptable instabilities of the RF fields in the cavities, which permit 10% rms variation of the peak beam current, are only about 0.01% rms in amplitude and 120 fs rms in phase according to beam simulation. The long-term RF variations can be compensated by feedback control of the RF amplitude and phase, the short-term or pulse-to-pulse variations, however, have to be reduced as much as possible by improving RF equipment such as amplifiers. Thus we have carefully designed and manufactured the RF cavities, amplifiers and control systems, giving the highest priority to the stabilization of the short-term variations..

STABILITY OF RF SYSTEM [3]

A 238-MHz SHB and an L-band correction cavity will be driven by solid-state amplifiers. An IOT (CPI/EIMAC CHK2800W) feeds an RF power of 120 kW to a 476-MHz booster. An L-band 30-MW klystron (E37612) was newly designed and manufactured by Toshiba Electron Tubes and Devices to drive the L-band APS type accelerating structures. A C-band correction accelerating structure will be driven by a C-band klystron (Toshiba E3748).

All the solid-state amplifiers adopt thorough stabilization countermeasures, such as temperature control with cooling water, employing a low-noise power supply and suppression of mechanical vibration in the chassis. LLRF instruments will be installed in air-conditioned (26±0.2˚C) 19'' enclosures. In order to suppress the RF phase drift of almost all of the transmission lines, such as coaxial cable and waveguides, the temperature of those transmission lines is controlled to 26±0.2˚C by using cooling water with a heat insulator.

All the above RF amplifiers, except for their control system and LLRF section, have been completed. Tolerances of RF fluctuation based on the beam analysis and achievements are summarized in Table 1.

Table 1: Tolerances and achievements for RF stability

	Tolerance (σ)		Measurement (std.)	
	Power	Phase	Power	Phase
SHB	0.02%	0.01˚	-	0.02˚
Booster	0.02%	0.02˚	0.026%	0.014˚ 1)
L-Correction	0.06%	0.06˚	0.052	0.062˚ 2)
L-APS	0.02%	0.06˚	Not yet	Not yet
C-Correction	0.2%	0.06˚	Not yet	Not yet

1) per 10 min., 2) per 1 mini.

L-BAND SYSTEM

The two L-band structures of APS (Alternative Periodic Structure) type will compress the 1 MeV beam bunch and accelerate it up to 35 MeV. An L-band (1428 MHz) klystron will generate an RF power of 20MW and the power will be divided to both structures via a directional coupler. A vacuum type waveguide circuit will be installed not to use insulation gases such as SF_6, that is, a circulator will not be available. Therefore the circuit has to be carefully designed to cancel the reflected powers from the APS's so that the reflection to the klystron will not cause RF instability in the klystron output cavity.

Accelerating Structure

The most important advantage of APS type comparing to a normal travelling wave structure are as follows: An APS type has an RF coupler, which results the field asymmetry, at around the center of accelerating structure, not at the entrance cell like a travelling wave type. Thus low energy beams just entering the structure do not get the emittance growth due to the field asymmetry and are accelerated up to the sufficient energy at around the coupler cell.

The structure is composed of two 1-m long accelerating structures and a central coupler cell brazed with the two structures. They have been very carefully machined, brazed and tuned to satisfy its specification.

The specifications and measured values of the important parameters are described in the following table.

Table 2: Parameters of Accelerating Structure

	Specification	Measurement#
Frequency	1428 ± 0.02 MHz	1428.000 MHz
Unloaded Q	> 20,000	24,300
Shunt Impedance	> 30 MΩ/m	32.8 MΩ/m
β	1.5 ± 0.1	1.45
Field Uniformity	95%	98.6%

The measurement was done only for APS-1.

Waveguide System

A simplified diagram of the waveguide system is presented in Fig 1. The dividing ratio of the directional coupler is supposed to be $r : 1-r$. A phase shifter installed in the downstream waveguide can adjust the RF phase (ϕ) for the downstream APS. RF powers reflected at the APS's are combined when those go through the directional coupler.

In case that the electric lengths of the waveguides from the directional coupler to the APS's are perfectly equal, the two APS's are completely the same and the phase shifter is ideal, the whole combined RF power is fed to an RF load and no reflection appears at the input port. Actual components, however, are not ideal, thus we have to evaluate tolerances of RF parameters.

In such a realistic case, the resonance frequencies of the APS's are not exactly equal to the operation frequency of 1428 MHz. The quality factors Q and the coupling coefficient β of each structure may have different values. All these realities will be taken into account to evaluate the RF reflection. Then we will especially know that the difference of the resonant frequencies has to be reduced as small as possible to minimize the reflection Γ_1.

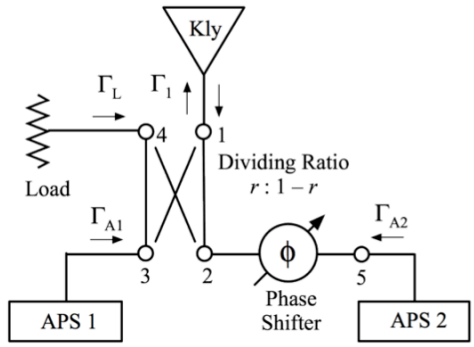

Figure 1: Simplified block diagram of L-band system.

When a step-function-like RF power is fed to such a realistic standing wave cavity, the transient backward voltage $V_b(t)$ is approximately expressed as follows:

$$V_b(t) \approx \left[\frac{2\beta}{1+\beta}\left(1+2jQ_L\frac{f-f_r}{f}\right)\left(1-e^{j\left(\pi f/Q_L\right)t}\right)-1\right]e^{j\omega t} \tag{1}$$

where f is the operation frequency, f_r is the resonant frequency of the APS and Q_L is the loaded Q of the APS.

According to the above equation, the backward RF power has the maximum value at $t = 0$, but it quickly decreases to around zero. The backward power increases again and reaches the saturated value at infinite time. We discuss about the reflection at the saturated condition in the following part.

Now we find the voltage reflection coefficient Γ at the input port of the APS-n:

$$\Gamma_{An} \approx \frac{2\beta_n}{1+\beta_n}\left(1+2jQ_{Ln}\frac{f-f_{rn}}{f}\right)-1 \tag{2}$$

An approximate expression of the voltage reflection at the input port of the directional coupler can be derived on the basis of the scattering matrix analysis:

$$\begin{aligned}\Gamma_1 \approx{}& \Gamma_h+\left(1+\Gamma_p\Gamma_{A2}\right)\Gamma_{A2}re^{-2j\phi}-(1-r)\Gamma_{A1}+r\Gamma_p\\ &-e^{-2j\theta}\Gamma_L r(1-r)\left[\left(1+\Gamma_p\Gamma_{A2}\right)\Gamma_{A2}re^{-2j\phi}+\Gamma_{A1}+\Gamma_p\right]^2\end{aligned} \tag{3}$$

where Γ_{An}, Γ_h and Γ_p are the voltage reflection coefficients of the APS's, the directional coupler and the phase shifter, respectively, and θ is the electric length from the port 4 to the APS-1.

In our case, the last term resulted by the reflection of the RF load is negligibly small. If the errors of r, β, Q and f_r are sufficiently small, the reflection Γ_1 can be approximately replaced with the total differential of the Equation 3 with respect to r, β, f_r, Q_L, Γ_p and ϕ:

$$\begin{aligned}\Gamma_1 \approx \Gamma_h &+ (\Gamma_{A2} + \Gamma_{A1})\delta r + \frac{\partial \Gamma_A}{\partial \beta}\left[r\delta\beta_2 - (1-r)\delta\beta_1\right] \\ &+ \frac{\partial \Gamma_A}{\partial f_r}\left[r\delta f_{r2} - (1-r)\delta f_{r1}\right] \\ &- \frac{\partial \Gamma_A}{\partial Q_L}\left[r\delta Q_{L2} - (1-r)\delta Q_{L1}\right] \\ &+ \left(\Gamma_A{}^2 + 1\right) r\Gamma_p - 2jr\Gamma_{A2}\phi\end{aligned} \quad (4)$$

The ideal r is 0.5. Thus Equation 4 is simply expressed as a linear function with respect to $\delta f_{r1} - \delta f_{r2}$, $\delta\beta_1 - \delta\beta_2$ and $\delta Q_{L1} - \delta Q_{L2}$. The term related with $\delta Q_{L1} - \delta Q_{L2}$ is also ignorable. Since the arguments of the complex Γ_h and Γ_p are unknown, we consequently suppose their arguments are $\pi/2$ on the polar coordinate given by Equation 1 to find the minimum tolerance of $\Delta f_{12} = \delta f_{r1} - \delta f_{r2}$. Table 3 presents the related tolerances providing $|\Gamma_1| < 0.1$ corresponding to the klystron's specified VSWR < 1.2 and measured values.

Table 3: Tolerances for $|\Gamma_1| < 0.1$

	Tolerance	Measurement
$\|\Gamma_h\|$	< 0.025	< 0.013
$\|\Gamma_p\|$	< 0.05	< 0.02
r	3 ± 0.1 dB	3 ± 0.08 dB
$\|\Delta f_{12}\|$	2.7 kHz	Not yet
$\|\Delta\beta_{12}\|$	0.2	Not yet
ϕ	± 7.5 deg.	± 7.5 deg

$\Delta f_{12} = \delta f_{r1} - \delta f_{r2}$ and $\Delta\beta_{12} = \delta\beta_1 - \delta\beta_2$

High Power RF Load [4]

We adopted a new type high power RF load proposed by Toshiba Corporation. The high power load is composed of an inlet waveguide with two stubs, an SiC hollow cylinder as an RF absorber and a water cooling jacket covering the SiC. A TE10 mode of microwaves transmitted to the load is transformed to a TE11 mode in the load chamber and absorbed by the cylindrical SiC in it. Now the completed load is waiting for a high power test.

Important features of this RF load are as follows.

- The RF load can stand for a high heat load because its cylindrical shape and a large heat jacket enable a good heat transfer from the SiC. When we dissipate a specified average power of 4.2 kW in the load, the maximum and average temperature in the SiC are expected to be about 45°C and 35°C, respectively.
- Since SiC's dielectric constant has temperature dependence, VSWR of the RF load varies as a function of the SiC's temperature. We therefore had to carefully determine the height of the stubs considering the realistic operation condition of the RF load.

GEOMAGNETIC ISSUE

The geomagnetic field slightly bend low energy electron beams, therefore this phenomena disturb fine beam tuning of the injector section. We therefore decided to introduce geomagnetic correction coils to cancel the geomagnetic field by a uniform magnetic field.

We recently surveyed the magnetic field at around the injector area in the accelerator tunnel before the construction of the injector. The measured data showed that the magnetic field strongly depended on positions and it suggested the geomagnetic correction would not function well.

The source of the inhomogeneous magnetic field was magnetism of the reinforcing steels in the RC floor. We demagnetized the floor using a flat square coils and its power supply with collaboration from Takenaka Corporation. The result of the demagnetization is shown in Fig. 2. The vertical components of the residual field with subtraction of the genuine geomagnetic field distribute in a range of 0 - 0.05 after the demagnetization, while -0.1 - 0.5 before it.

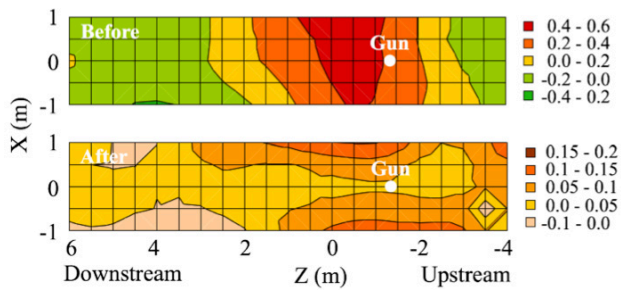

Figure 2: The vertical magnetic field distribution on the horizontal plane at the height of the beam (80 cm) in the injector area before/after the demagnetization. The geomagnetic components are subtracted.

REFERENCES

[1] T. Shintake, "Status Report on Japanese XFEL Construction Project at SPring-8", in these proceedings.

[2] K. Togawa et al., "CeB_6 electron gun for low-emittance injector", PR STAB, 10, 020703 (2007).

[3] T. Asaka et al., "Development Status of RF System of Injector Section for XFEL/SPring-8", in these proceedings.

[4] J. Watanabe et al., "Duct-Shaped SiC Dummy Load of L-band Power Distribution System for XFEL/SPring-8", in these proceedings.